Climate Dynamics (2001) 17: 327–338

Y. M. Liu · G. X. Wu · H. Liu · P. Liu

Condensation heating of the Asian summer monsoon and the subtropical anticyclone in the Eastern Hemisphere*

Received: 10 September 1999 / Accepted: 5 June 2000

Abstract The effects of condensation heating on the formation of the subtropical anticyclone in the Eastern Hemisphere (EH) are studied by means of theoretical analysis and numerical simulation. The complete vorticity equation is employed for the analysis. It is found that, due to the vertical gradient of strong condensation heating, the distribution of cyclone and anticyclone in the upper troposphere is out of phase with that in the middle and lower troposphere. This is confirmed by a series of numerical experiments. The horizontal gradient of the condensation heating also affects the configuration of the subtropical anticyclone. It is concluded that condensation heating is a key factor for the formation and location of the summer subtropical anticyclone in the EH. The latent heating released by the Asian monsoon rainfall contributes to the formation of the 200 hPa South Asian anticyclone on the western side of the heating center and the 500 hPa western Pacific subtropical anticyclone on the eastern side of the center. Such configurations are modified to some extent by surface sensible heating and orography. The circulation in mid-latitudes is also affected by the latent heating in the subtropical area through the propagation of Rossby waves.

1 Introduction

In the boreal summer, the atmospheric circulation over East Asia is characterized by the existence of two persistent subtropical anticyclone systems. One is the pronounced South Asian anticyclone (SAA) in the upper troposphere just over the region to the north of the Bay of Bengal; and the other, the subtropical anticyclone over the western Pacific (SAWP). The seasonal variations of these two systems are closely linked to the onset and withdrawal of the Asian summer monsoon. Their spatial and temporal variations are associated not only with the disastrous weather in the area, such as typhoons and torrential rain, but also with severe climate anomalies, such as drought and flooding over vast areas. The formation and evolution of these two systems, therefore, have long been the subjects of atmospheric studies (e.g., Krishnamurti 1973; Peng 1987; Zhang et al. 1995).

After early spring, the strong elevated surface sensible heating of the Tibetan Plateau persistently warms up the air column aloft at a rate of 2 to 4 °C per day (Ye and Gao 1979; Wu and Zhang 1998). Vigorous ascent of the air column over the Tibetan Plateau due to such surface sensible heating then sucks the surrounding air from below and expels it outwards in the upper layer, acting as an air-pump. Since the air-pump is mainly driven by surface sensible heat flux, it was defined as the sensible heat driven air-pump, or SHAP (Wu et al. 1997a). The SHAP generates the near surface positive vorticity and upper-layer negative vorticity, and regulates the atmospheric circulation in the area. These together with its mechanical forcing are essential in maintaining the huge upper-layer anticyclone with a warm and moist core (Ye et al. 1957; Flohn 1957; Ye and Wu 1998). However, the anticyclone generated in such a way in the upper troposphere is mainly over the Plateau, and usually named the Tibetan anticyclone. Its location is somewhat to the north of the SAA center. It accounts only a part of the formation of the SAA. In addition numerical experiment results of Li and Luo (1988) show that the moisture processes can enhance the SAA and the development of meridional flow. These provide the evidence that there must be another mechanism that links the formation and maintenance of the SAA to the condensation heating in the monsoon area. The search for such mechanism concerns the current study.

* This paper is a contribution to the AMIP-CMIP Diagnostic Subproject on General Circulation Model Simulation of the East Asian Climate (EAC), coordinated by W.-C. Wang

Y. M. Liu (✉) · G. X. Wu · H. Liu · P. Liu
State Laboratory of Numerical Modeling for
Atmospheric Sciences and Geophysical Fluid Dynamics (LASG)
Institute of Atmospheric Physics, Chinese Academy of Sciences,
Beijing 100029, China
E-mail: lym@lasg.iap.ac.cn

Most of the studies on the SAWP at 500 hPa were devoted to its impacts on the surrounding weather and climate (e.g., Huang and Yue 1962; Tao and Chen 1987; Samel et al. 1999). Nitta (1987) conducted a correlation analysis and found that there is a wave train of geopotential height, which emanates from the heat source region near the Philippines and propagates through Japan to North America. This wave train appears to be generated when convective activities over the Philippine Sea become intense. Huang and Li (1989) further showed that during the northward propagation of these quasi-stationary planetary waves the SAWP shifts northward and intensifies. Despite these great efforts the mechanism of the formation of the SAWP and its anomaly is still unclear in general. It is, however, interesting to notice that the movement of the SAA and that of the SAWP are not separated. The study of Tao and Zhu (1964) indicates that the eastward migration of the 100 hPa SAA is usually followed by the westward movement of the 500 hPa SAWP. This then suggests the existence of some common mechanism that links the movement of one system to the other.

Traditionally, the existence of subtropical anticyclones is thought to be attributed to the radiative cooling and sinking of the descending arm of the Hadley circulation (Peixoto and Oort 1991). However, the zonal-mean Hadley circulation shows very strong descent during winter, whereas the summer subtropical anticyclones are in most measures stronger as well as more longitudinally extended than their winter counterparts. As pointed out by Hoskins (1996), the classical Hadley-cell theory does not work well for the formation of the summer zonal mean anticyclone belt.

This is also the case even in three-dimensional space. For example, in the lower troposphere in July, the subtropical anticyclones are over the North Pacific and North Atlantic (Fig. 1c), whereas the descending centers appear over their eastern parts (Fig. 1b). In contrast ascending motion prevails over the western parts of these anticyclones. At 500 hPa, in the western parts of the SAWP and the subtropical anticyclone over North America (Fig. 1a), ascending motions dominate as well. It is clear that for the formation of subtropical anticyclones, the classical descent theory is quite limited both in the zonal mean and three-dimension cases.

In fact, anticyclone formation can be interpreted in terms of the development of negative vorticity. The latter is associated with the fluid divergence, i.e.,

$$\frac{\mathrm{d}\zeta}{\mathrm{d}t} \propto -(f+\zeta)\nabla\cdot\vec{V} \tag{1}$$

From the continuity equation and state equation

$$\nabla\cdot\vec{V} = \frac{1}{\alpha}\frac{\mathrm{d}\alpha}{\mathrm{d}t} = -\frac{1}{p}\frac{\mathrm{d}p}{\mathrm{d}t} + \frac{1}{T}\frac{\mathrm{d}T}{\mathrm{d}t} \tag{2}$$

the compression of a descending parcel can only result in its convergence. It is the adiabatic warming of the descending parcel that contributes to its divergence. These

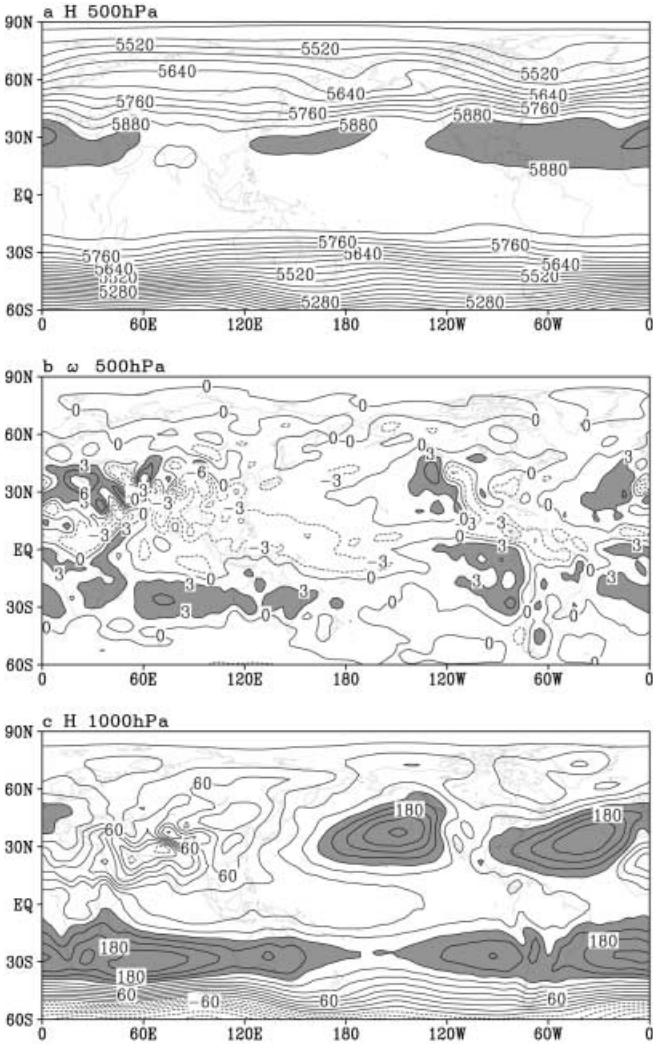

Fig. 1a–c The distributions of the July mean geopotential height at **a** 500 hPa and **c** 1000 hPa and **b** ω at 500 hPa calculated from the NCEP/NCAR reanalysis data for 1980–95. The contour intervals are 40 gpm in **a**, $3 * 10^{-2}$ Pas^{-1} in **b**, and 20 gpm in **c**

effects on the vorticity variation are described by the corresponding terms in the following equation

$$\frac{\mathrm{d}\zeta}{\mathrm{d}t} \propto (1-\kappa)(f+\zeta)\frac{\omega}{p} - (f+\zeta)\frac{1}{\theta}\frac{\mathrm{d}\theta}{\mathrm{d}t} \quad . \tag{3}$$

Thus, the descent itself can only produce **positive** vorticity. Only due to the adiabatic warming of the descending parcel can **negative** vorticity be forced. Assume that an air parcel descends adiabatically from 400 hPa to 800 hPa and its average temperature is 250 K. Then the ratio between the two terms on the right hand side of Eq. (2) is estimated to be 10:3. Therefore adiabatic descent as a whole cannot explain the development of anticyclone vorticity. New mechanisms for the formation of the subtropical anticyclone need to be explored.

Rodwell and Hoskins (1996) proposed a monsoon-desert mechanism for subtropical desertification by which remote diabatic heating in the Asian monsoon region can induce a Rossby wave pattern to the west,

and contribute to the formation of the in situ desert climate, including the lower layer subtropical anticyclones. This work helps explain subtropical dynamics. However, the diabatic heating used in their study was obtained from analysis data as a residual of the thermodynamic equation. This makes it difficult to distinguish the contributions of latent heating to the formation of the subtropical anticyclone from the other kind of diabatic heating. To overcome the limitation, in this study we use the condensation heating of the Asian monsoon rainfall as a unique forcing to investigate the atmospheric response.

The dynamics of low-frequency structure vary greatly with latitude. Hoskins (1986) used the Burger number B $(=N^2H^2/f^2L^2)$ to gain new insights into observed atmospheric behavior. For large-scale motions in the subtropics, B is of order unity so that both horizontal and vertical advection must be retained in the thermodynamic equation when subtropical anticyclone formation is considered.

In a series studies Wu et al. (Wu and Liu 1998; Wu et al. 1999; Liu et al. 1999) have deduced a complete vorticity equation (CVE) and showed that the CVE is exactly equivalent to the Ertel potential vorticity equation (Ertel 1942). The CVE includes explicitly dynamical as well as thermodynamical elements, such as frictional dissipation and diabatic heating, and is appropriate for our present study. The equation can be expressed as

$$\begin{aligned}&\dot{\zeta}_z + \beta v + (f+\zeta_z)\nabla\cdot\vec{V}\\ &\quad = -\rho[(P-\xi_s\theta_s)\theta_z^{-2}\dot{\theta}_z + \xi_s\theta_z^{-1}\dot{\theta}_s + \theta_s\theta_z^{-1}\dot{\xi}_s^{-1}]\\ &\qquad + \theta_z^{-1}(\vec{F}_\zeta\cdot\nabla\theta + \vec{\zeta}_a\cdot\nabla Q), \quad (\theta_z\neq 0) \end{aligned} \tag{4}$$

where $\vec{\zeta}_a$ is a three dimensional absolute vorticity, ζ_z is the vertical component of $\vec{\zeta}_a$ and $\dot{A}$, the substantial derivative of A. The terms on the right-hand side of the above equation indicate, respectively, how the changes in static stability (θ_z), baroclinity (θ_s), vertical wind shear (ξ_s), frictional dissipation $(\vec{F}_\zeta)$ and diabatic heating (Q) affect the development of vertical vorticity. When only the forcing of diabatic heating is concerned, Eq. (4) becomes

$$\begin{aligned}&\frac{\partial\zeta_z}{\partial t} + \vec{V}\cdot\nabla\zeta_z + \beta v\\ &\quad = (1-\kappa)(f+\zeta_z)\frac{\omega}{P} - (f+\zeta_z)\frac{1}{\theta}\frac{\mathrm{d}\theta}{\mathrm{d}t} + \frac{f+\zeta_z}{\theta_z}\frac{\partial Q}{\partial z}\\ &\qquad - \frac{1}{\theta_z}\frac{\partial v}{\partial z}\frac{\partial Q}{\partial x} + \frac{1}{\theta_z}\frac{\partial u}{\partial z}\frac{\partial Q}{\partial y}, \quad \theta_z\neq 0\ . \end{aligned} \tag{5}$$

A scaling analysis shows that the vorticity variation forced by vertically inhomogeneous heating is stronger than that by horizontally inhomogeneous heating. The order of magnitude of the other terms on the right hand side of Eq. (5) is smaller (10^{-11}) than that generated by the vertical variation of diabatic heating (10^{-10}). Thus during a very short period of time,

$$\frac{\partial\zeta_z}{\partial t} \propto \frac{f+\zeta}{\theta_z}\frac{\partial Q}{\partial z}, \quad \theta_z\neq 0\ . \tag{6}$$

Along the ridge of the subtropical anticyclone, zonal winds are very weak ($u\sim 0$), and for an initially zonal flow, the meridional winds are negligible, then the horizontal advection term in the vorticity Eq. (5) is very small. This is true particularly in the case of intense deep-convective heating since such heating produces strong westerly to its north and easterly to its south. Thus in a steady state, Eq. (5) can be simplified as

$$\beta v \propto \frac{f+\zeta}{\theta_z}\frac{\partial Q}{\partial z}, \quad \theta_z\neq 0\ . \tag{7}$$

Therefore a zonally symmetric anticyclone belt will be disturbed by the diabatic heating, with the resultant pattern depending upon the vertical profile of the heating.

In this study, based upon the theoretical analysis outlined, we focus on the effects of condensation heating associated with the Asian summer monsoon on the nature of isolated subtropical anticyclone by using numerical simulations. The work is organized in six sections. The model description will be presented in the next section. In Sect. 3 the effects of an idealized condensation heating on a zonally symmetric subtropical circulation are discussed. In Sect. 4 such effects are further examined by introducing more realistic condensation heating and using a series of perpetual July experiments. The comparison of effects between condensation heating and sensible heating is also explored in this section. Section 5 presents an analysis of the relationship between the interannual variation of the condensation heating and subtropical circulation in the Asian monsoon area. Conclusions and discussion are presented in Sect. 6.

2 Model

The model used in this investigation is the Global Ocean-Atmosphere-Land System Climate Model developed at LASG of the Institute of Atmospheric Physics (IAP), i.e., the IAP/LASG GOALS (Wu et al. 1997b). The atmospheric component is a 9-layer spectral model in σ-coordinate, which in the horizontal direction is rhomboidally truncated at zonal wave number 15 (Wu et al. 1996). Its dynamic framework uses a 'standard atmosphere reduction' scheme (Zeng 1963; Phillips 1973). The radiation scheme absorbed in the model is an extension of the k-distribution (or ESFT, the exponential sum fitting of transmission function) representation of the atmospheric gaseous absorption developed by Shi (1981) and Wang (1996). The convection and condensation processes are parametrized by using the dry/moist convective adjustment (Manabe et al. 1965). The land surface process implemented in the GOALS is the SSiB model (Xue et al. 1991; Liu and Wu 1997). The ocean component of the GOALS is a 20-layer oceanic general circulation model developed by Zhang et al. (1996).

For the present study, the ocean component is switched off, and the model is integrated over 20 years with prescribed climate mean SST and sea ice, which are produced from the data set of the Atmospheric Model Intercomparison Program (AMIP). This integration is then defined as the control (CON) run. In general, IAP/LASG GOALS model is able to reproduce the current observed climate reasonably, especially for the large-scale features

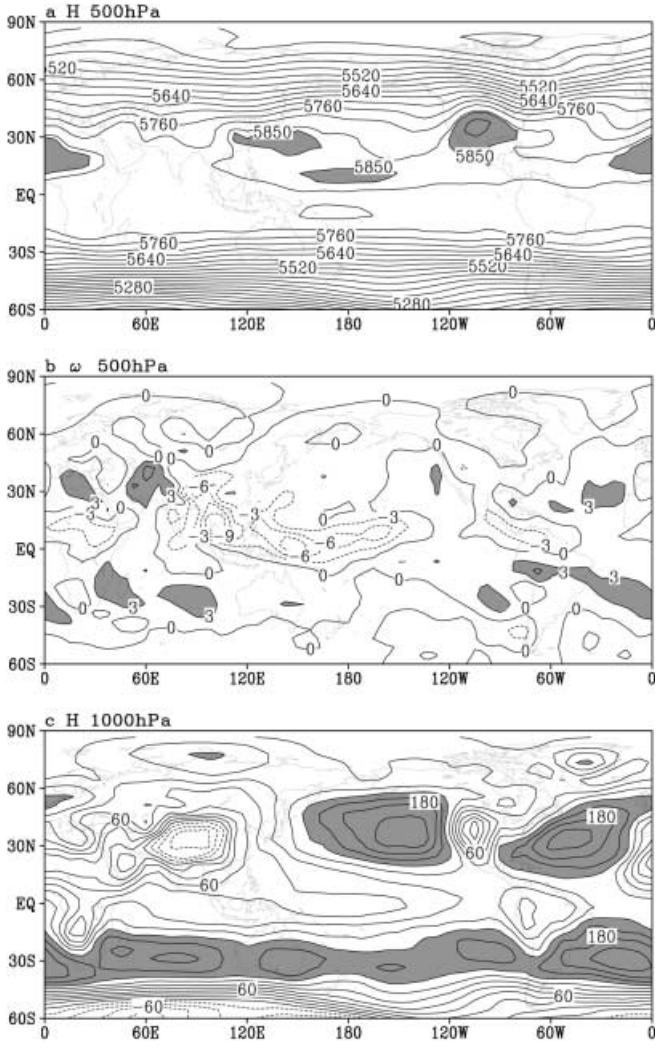

Fig. 2a–c The same as Fig. 1, but for the results derived from the IAP/LASG GOALS climate model and averaged over a 16-year period

and seasonal cycle. Figure 2 shows the circulation derived from the last 16-year integration results. Compared with Fig. 1, it can be seen that the space distributions of the subtropical anticyclones and vertical velocity are simulated reasonably well. The general features of the subtropical anticyclones over the western Pacific, Northern America, and northern Africa at 500 hPa (Fig. 2a), the two low-level oceanic anticyclones at 1000 hPa (Fig. 2c), and the ascendant motion over the western parts of the 1000 hPa subtropical anticyclones are similar to the reanalysis results (Fig. 1). The apparent discrepancy in depicting the observed climate is over the equatorial middle-Pacific, where the simulated geopotential height is too low at 1000 hPa and too high at 500 hPa, and the rate of ascent over the region is too strong.

3 Condensation heating and the subtropical anticyclones

In the real world, the atmospheric response to condensation heating may also be affected by other factors, such as orography and sensible heating etc. A better understanding of the problem is sought in this section through idealized experiments. No orography is used in such an experiment and an aqua-planet is assumed. The condensation heating generated by the model adjustment and the global surface sensible heating, which will be diffused into the free atmosphere, have been turned off in the thermodynamic equation. Instead, an idealized "monsoon" heating, which mimics the three-dimensional condensation heating distribution over the Bay of Bengal as obtained from the NCEP/NCAR reanalysis data, is introduced into the model integration. The boxes shown in Fig. 3 indicate the elliptical region where such heating is more than 1 K day^{-1} at its maximum vertical level ($\sigma = 0.336$). It is centered at 90°E and 20°N. The vertical profile of this heating is shown by the shaded region in Fig. 4d, with a maximum of 8 K day^{-1} at about 336 hPa representing what is observed from the reanalysis data. To concentrate on the summer circumstances, the solar azimuth is set by its value on July 15 throughout the experiment. With the zonal-mean July circulation obtained from the CON run as initial conditions, this perpetual July experiment has been run for 24 months in total and defined as LH1 experiment in the following contexts.

3.1 Transient response

According to Eq. (6), in an inertially and statically stable atmosphere in which $f + \zeta > 0$ and $\theta_z > 0$, the vorticity generated by a latent heating (Q_{LH}) above its maximum heating level z_M can be expressed as,

$$\frac{f+\zeta}{\theta_z}\frac{\partial Q_{LH}}{\partial z} < 0, \quad \theta_z \neq 0, \ z > z_M \tag{8}$$

anticyclone vorticity is thus produced above z_M, whereas cyclone vorticity is produced below z_M. In experiment LH1, the forced horizontal wind vector and vorticity are plotted in Fig. 3. At day 1 in the upper troposphere, an anticyclone with negative vorticity and divergence appear above the heating area (Fig. 3a). The vorticity center enhances strongly and shifts westward with time. At day 4, the central perturbation vorticity is about $18 * 10^{-6}$ s^{-1}, three times as strong as that at day 1. Besides this local effect, the heating also generates a westward-moving Rossby wave solution with a phase speed of about 12° longitude per day, in good agreement with the analytical results of Gill (1980) and Rodwell and Hoskins (1996).

The perturbations at the lower level (Fig. 3b, d) show a reverse response to those at the upper level (Fig. 3a, c). Cyclones appear at the lower level. In addition, at either the higher level or lower level around the heating boundary, perturbation vorticity is opposite to that within the heating source. This means the condensation heating can generate a compensatory circulation in the neighborhood. Nevertheless, the transient perturbation is localized during a very short time scale.

3.2 Stationary response

For a steady state and below the maximum heating level z_M, Eq. (7) becomes

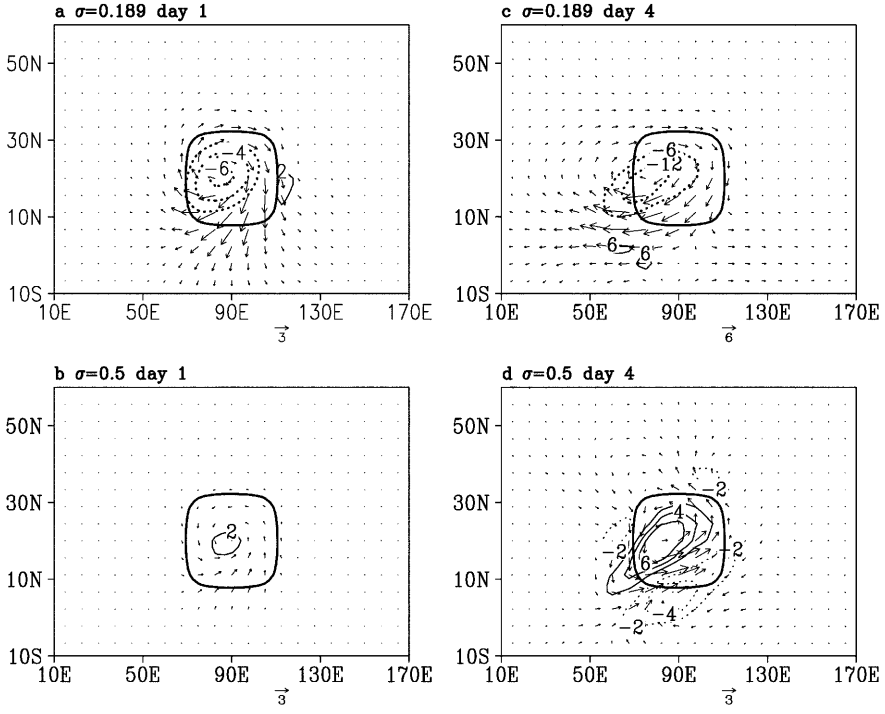

Fig. 3a–d The perturbation vorticity (*isoline*) and horizontal winds (*vector*) generated in the experiment LH1 **a**, **b** at day 1, and **c**, **d** day 4 of the integration. **a** and **c** present the distribution at $\sigma = 0.189$; **b** and **d**, at $\sigma = 0.5$. Contour interval is $2 * 10^{-6}$ s^{-1} in **a**, **b** and **d**, $6 * 10^{-6}$ s^{-1} in **c**. The unit of the wind vector *below each panel* is m s^{-1}. The *boxes* indicate heating region of more than 1 Kd^{-1} at $\sigma = 0.336$

$$\beta v \propto \frac{f+\zeta}{\theta_z}\frac{\partial Q_{LH}}{\partial z} > 0, \quad \theta_z \neq 0, \ z < z_M \tag{9}$$

and southerlies are therefore forced. A low-level subtropical cyclone center then appears on the western side of the deep condensation heating; but an anticyclone center appears on the eastern side of the deep condensation heating. Above the maximum heating level, Eq. (7) becomes

$$\beta v \propto \frac{f+\zeta}{\theta_z}\frac{\partial Q_{LH}}{\partial z} < 0, \quad \theta_z \neq 0, \ z > z_M \tag{10}$$

and northerlies are forced. An anticyclone center then appears on the western side of the deep condensation heating.

In using the GOALS model, a numerical experiment usually reaches its equilibrium after six months' integration. In order to investigate the steady response to condensation heating, the outputs derived from the last 12 months' integration of LH1 are averaged and shown in Fig. 4. Here the values of geopotential height are subtracted by their zonal mean. At the upper troposphere levels (Fig. 4a, b), high pressure appears on the western side of the heating source, and low pressure appears on its eastern side. At the lower troposphere level (Fig. 4c), the pressure pattern is reversed. High pressure appears on the eastern side of the heating source, and low pressure appears on its western side. The vertical distribution of the stream function (Fig. 4d) is in good agreement with our theoretical analysis: it is due to the vertical gradient of condensation heating that the forced circulation displays a reverse phase between the upper and lower troposphere. This result is also in accordance with the numerical results of Hoskins and Karoly (1981) for a deep elliptical heat source at 15°N perturbing the Northern Hemisphere winter zonal flow.

Usually, it merits careful attention to conduct such an idealized experiment because of the multi-scale nature of the atmospheric system and the scale-interaction issues. For the present study, these are not the major concern since the dynamics involved is mainly linear. As stated by Eq. (7), the response of the meridional wind (v) to the forcing $S(=\frac{f+\zeta}{\theta_z}\frac{\partial Q}{\partial z})$ is roughly linear, i.e., $v \propto \lambda S$. Then each component of the source spectrum will force an in-phase v-component. Therefore, for a stationary atmosphere, the forced strongest southerly/northerly flow should always be located just below/above the heating center, as shown in Figs. 4a–c and 5a, b.

An important phenomenon appears in these experiment results: although the maximum southerly at the lower level and northerly flow at the upper level are forced within the heating region as anticipated from Eqs. (9) and (10), the prominent maximum response in geopotential height is not located at the latitudes where the heating is imposed, but to its north. Furthermore, along these maximum response latitudes, the highs are stronger than the lows and an anticyclone center appears just at the northern rim of the heating region at both lower and upper levels (Fig. 4a–c). This is because an appendant negative vorticity forcing is generated to the north of the heating region by horizontal inhomogeneous heating. In fact, by using the thermal wind relation, the last two terms in Eq. (5) can be written as

$$\left(\frac{\partial \zeta_z}{\partial t}\right)_x^Q \propto -\frac{g}{fT\theta_z}\frac{\partial T}{\partial x}\frac{\partial Q}{\partial x},$$

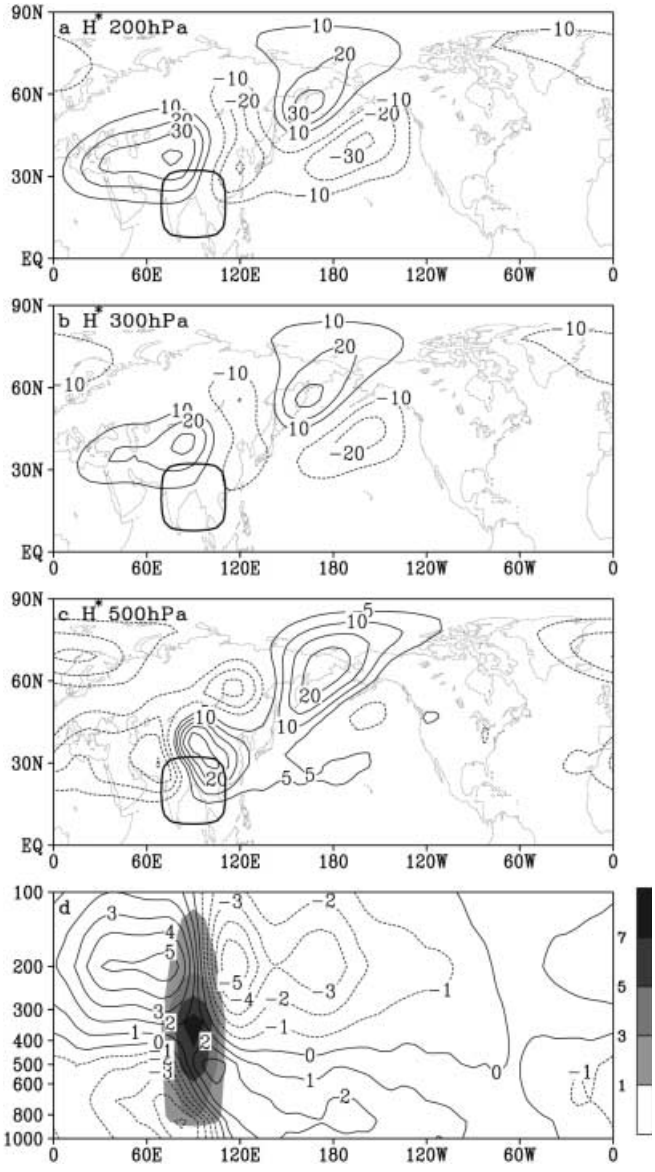

Fig. 4a–d Average fields of the last 12-month results from the idealized experiment LH1. **a**–**c** Deviation of geopotential height from zonal mean at 200, 300 and 500 hPa, respectively. The contour interval is 10 gpm in **a** and **b**, and 5 gpm in **c**. The *boxes* are as in Fig. 3. **d** Vertical cross section of stream function at 30°N, contour interval is $1 * 10^{-6}$ m^2 s^{-1}. The *shaded area* in **d** displays the profile of condensation heating at 20°N, and the *contours* denote 1, 3, 5, 7 Kd^{-1}, respectively

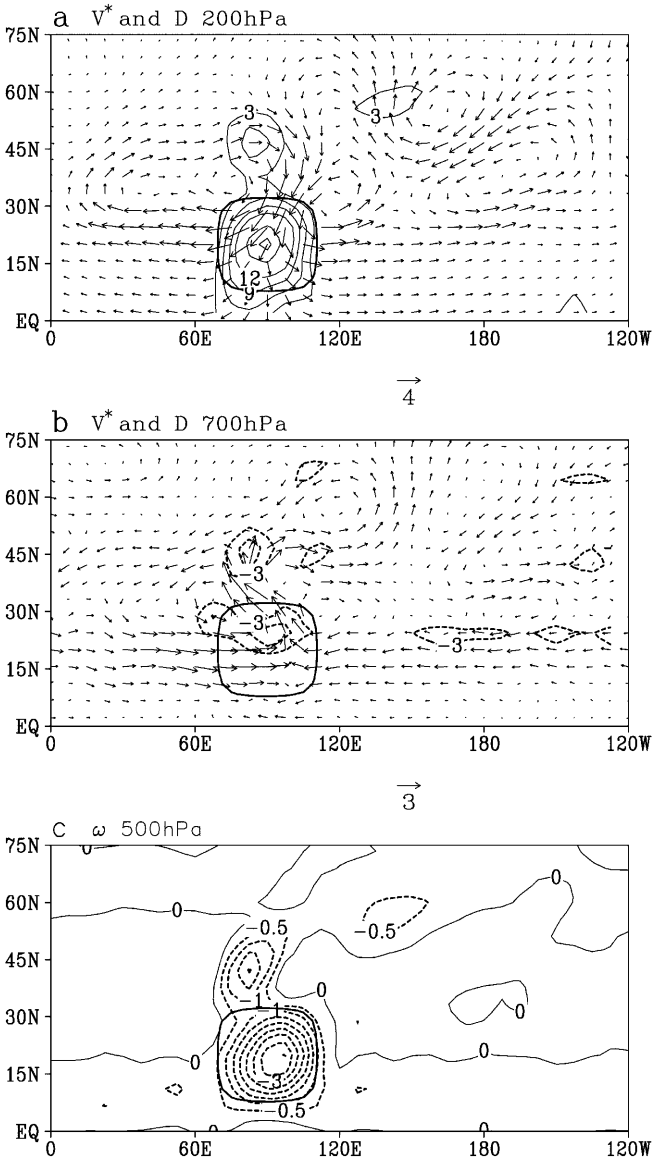

Fig. 5a–c Average fields of the last 12-month results from the idealized experiment LH1. **a**, **b** Wind vector deviation from zonal mean (ms^{-1}) and divergence (D, *isoline*) at 200 and 700 hPa, respectively; the contour interval is $3 * 10^{-7}$ s^{-1}; *solid curves* denote divergence, and *dashed*, convergence. **c** ω at 500 hPa. The contour interval is $0.5 * 10^{-2}$ Pas^{-1}. The *boxes* are as in Fig. 3

$$\left(\frac{\partial \zeta}{\partial t}\right)_y^Q \propto -\frac{g}{fT\theta_z}\frac{\partial T}{\partial y}\frac{\partial Q}{\partial y} \quad . \tag{11}$$

Therefore within the heating region as well as in the surroundings, as the air column over the heating region is warmed up, the horizontal gradient of temperature is in phase with that of the diabatic heating and negative vorticity is produced. According to Eq. (5) outside the heating region, $\frac{f+\zeta_z}{\theta_z}\frac{\partial Q}{\partial z} = 0$. Thus at the upper level of the northern rim of the heating region, the westerly flow turns southward towards the heating region, causing divergence to its north just between the mid-latitude westerly to the north and the northwesterly to the south (Fig. 5a). At a lower level, the southerly flow within the heating region is also subject to such negative vorticity forcing. It turns clockwise, leaves the heating region and merges into the mid-latitude westerly, forming low-level convergence just below the upper-level divergence (Fig. 5b). As a result, vertical-ascending motion with a velocity as high as $2 * 10^{-2}$ Pas^{-1} is forced (Fig. 5c). This ascent becomes a strong negative vorticity source with an intensity of 10^{-11}–10^{-10} s^{-2} (Eq. 5). Consequently, such negative vorticity together with the vorticity generated by the vertically inhomogeneous

diabatic heating make the anticyclone more powerful and larger in size than the cyclone in the heating area and that to its north (Figs. 4a–c, 5a, b). This is the reason why the vertical cross section chosen for Fig. 4d is along 30°N, rather than across the heating center at 20°N.

3.3 Propagation of stationary wave

In Figs. 4a–c and 5a, b it is clearly shown that, besides the responses on the eastern and western sides of the heating region, there exists an equivalent barotropic Rossby wave train emanating from the heating region and propagating northeastwards. The positive center is located around the Kamchatka Peninsula, and the negative centers are located over the Lake Baikal and the eastern Pacific.

To explain such wave propagation, the initial zonal wind and its variation due to the diabatic heating are shown in Fig. 6. The initial zonally symmetric wind U^0 is shown in Fig. 6a. The prescribed heating is located at the junction between the westerly to the north and the easterly to the south. The zonal wind variation U^* shown in Fig. 6b indicates that in the middle and upper troposphere, westerly winds increase to the north of heating region, while easterly winds increase to its south. As a result, the condensation heating strengthens the westerly jet to the north and the easterly jet to the south so that in the heating region the advection is weak. This then justifies our previous simplification by which Eq. (7) was obtained.

Corresponding to the appendant negative vorticity forcing as discussed in Sect. 3.2, horizontal anticyclonic shear appears to the south of about 50°N (Fig. 6b). Figure 6b also shows that, due to the horizontal convergence in the lower layers, cyclone vorticity exists near the surface not only in the heating region, but also to its north. This cyclone vorticity weakens with height, and at about 400 hPa, changes to the aforementioned anticyclone circulation. Within the heating region, however, the effect of the horizontally inhomogeneous heating is much weaker than the vertically inhomogeneous heating. Thus, the major feature of the forced circulation is similar to that caused by the vertically inhomogeneous heating.

To understand the behavior of wave propagation, the distribution of the 'critical stationary wave number' K_s defined by Hoskins and Karoly (1981) is analyzed. According to their theory, Rossby waves propagate towards larger values of K_s, and are trapped in the area of easterlies ($\bar{u} < 0$). Figure 6d shows the distribution of the 'critical stationary wave number' K_s calculated from the zonal wind shown in Fig. 6c (here $\bar{u} = U$). It indicates that Rossby waves can propagate northward from the heating source into the mid-high latitudes, and explains why there are Rossby wave trains in Figs. 4 and 5.

The height of 300 hPa is close to the height of maximum heating (336 hPa) where $\frac{\partial Q_{LH}}{\partial z} = 0$. Therefore, the geopotential height deviation from zonal mean is not conspicuous at 300 hPa compared with those at 200 hPa or 500 hPa, thus the wave train is observed more clearly

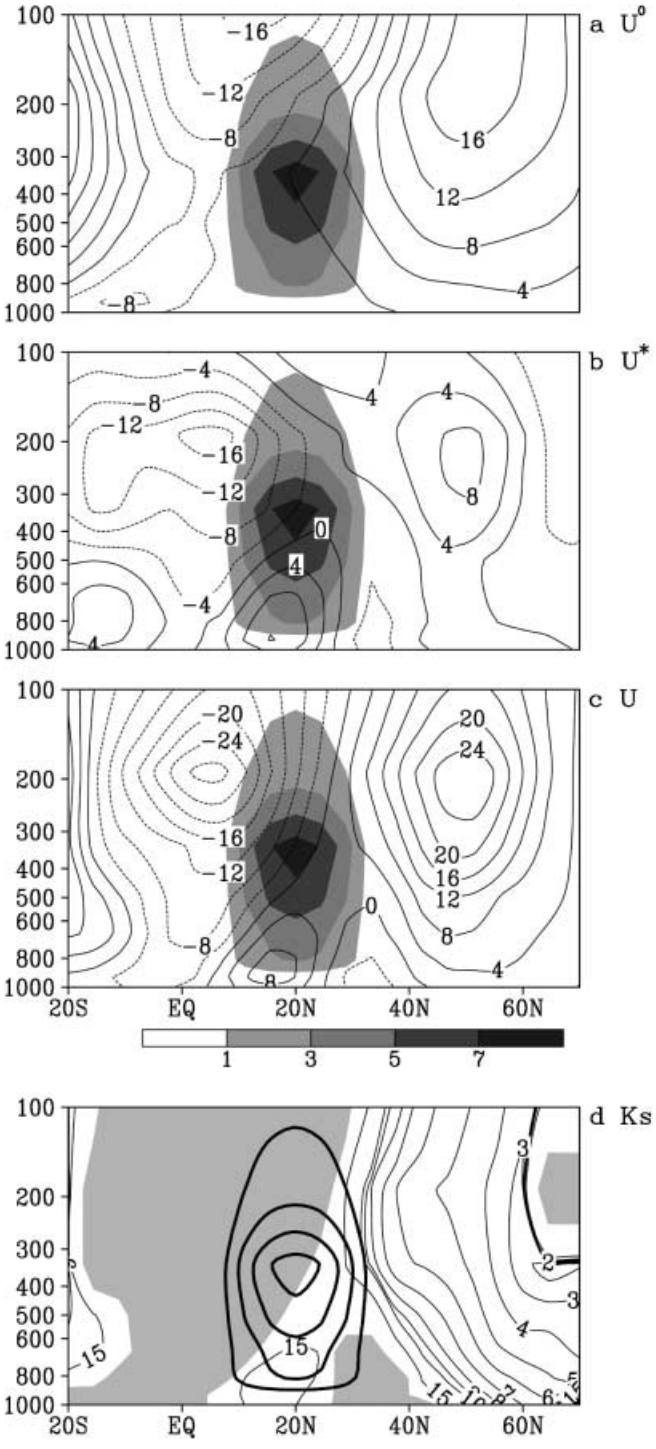

Fig. 6a–d North-south vertical sections across the heating center (90°E) in the idealized LH1 experiment of **a** the initial zonal wind U^0, **b** the variation of zonal wind U^* after the condensation heating is turned on, **c** the total zonal wind U ($U = U^0 + U^*$) averaged over the last 12 months, and **d** the critical stationary wave number K_s (see text for details). The *shaded area* in **a–c** and the *bold curves* in **d** are the same as in Fig. 4d

(Fig. 4b). In higher latitudes, the wave train shown in Fig. 4a–c and Fig. 5a, b is equivalent to barotropic in structure, a result of the 'advective' limit as discussed by Smagorinsky (1953). This means that the circulation pattern in mid-high latitudes, such as blocking anticyclones, may be affected by the condensation heating in the subtropical region.

4 The effects of July condensation heating on subtropical anticyclones

The results in the last section show that the subtropical anticyclones can result from an idealized condensation heating at the subtropics. To make the study closer to reality, in this section a prescribed forcing of the July condensation latent heating is derived from the control experiment (CON) and saved at each grid point of the model. This forcing is considered as a 'real model heating', and the atmospheric responses to the forcing is investigated in the following experiments.

4.1 Responses of zonal symmetric circulation to the 'real' latent heating without orography

Another perpetual July experiment LH2 is designed for the present purpose. As used in the idealized experiment LH1 presented in Sect. 3, in LH2, no orography is used and surface sensible heating is turned off. Initiated with the same zonal-mean July circulation as in LH1, this perpetual July experiment (LH2) is also integrated for 24 months. Similarly, the results averaged over the last 12 months are employed for the following analysis.

The plot of precipitation shown in Fig. 7a reflects the distribution of vertically integrated heating. The result shows that, in the subtropics of the EH, the monsoon rainfall area of more than 2 mm d^{-1} covers the area from the eastern Tibetan Plateau to the west of the dateline.

The steady responses of geopotential heights in LH2 (Fig. 7b, c) are similar to those in LH1. At 200 hPa along 30°N, there are positive height deviations to the west of the heating, ranging from the Tibetan Plateau to the lower reaches of the Yangtze River with a maximum as high as 80 gpm. The negative height is over the central and eastern Pacific with a center of −60 gpm. Similar to Fig. 4a–c, a Rossby wave excited by the heating propagates northeastward. In mid-high latitudes, it is still equivalently barotropic in nature, but twice as strong as that in Fig. 4. Moreover, the response centers shift eastward compared with those in LH1. Such results are related to the fact that in LH2, the latent heating is larger around 90°E, and the region of the heating shifts eastward as well. At 500 hPa, the pattern in the subtropics is opposite to that at 200 hPa. In the western Pacific, the high pressure appears to the east of the condensation heating with a value of 20 gpm. On the other hand, in a contrasting experiment in which the condensation heating is removed, there is only an almost zonal symmetric high belt over the subtropics at each level (figures not shown).

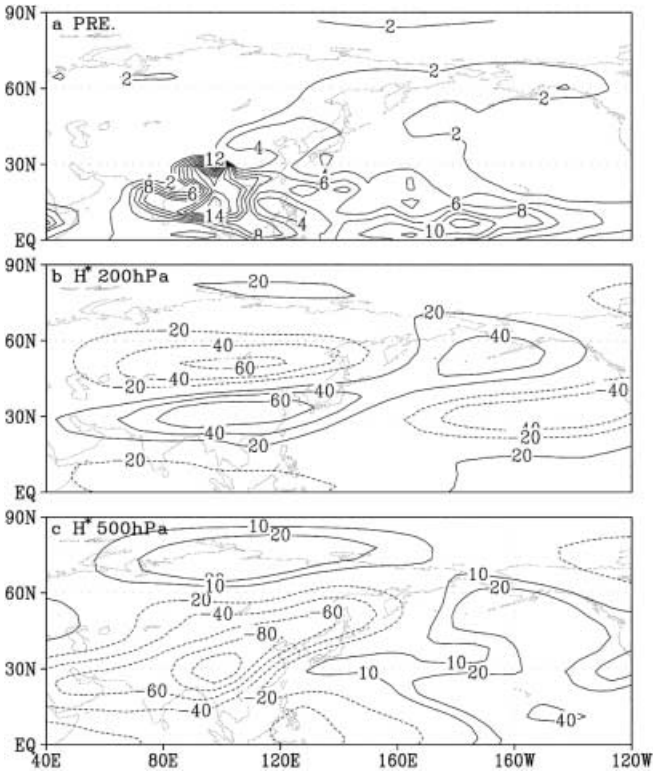

Fig. 7a–c Average fields of the last 12 months' results obtained from the experiment LH2. **a** Precipitation, contour interval is 2 mm d^{-1}. **b**, **c** show the deviations of geopotential height (gpm) from the corresponding zonal means at 200 hPa and 500 hPa, respectively

It is clear that the prescribed July condensation heating can break the zonal symmetric anticyclone belts into isolated anticyclones and cyclones. It contributes to the formation of the SAA and tropical upper-tropospheric trough (TUTT) in the upper troposphere (200 hPa) and the SAWP in middle troposphere (500 hPa).

4.2 Responses of zonal symmetric circulation to latent heating with orography

The next experiment (LH3) is almost the same as LH2 but with orography included during the integration. The height deviation and condensation heating shown in Fig. 8a indicate that with the orography and land-sea distribution included the subtropical anticyclone in the middle and lower troposphere and the SAA in the upper troposphere can be produced to a reasonable extent by condensation latent heating alone. These results are consistent with the theoretical analysis presented in Sect. 1, and with the results from the idealized latent heating experiment LH1 and the model-prescribed latent heating experiment LH2.

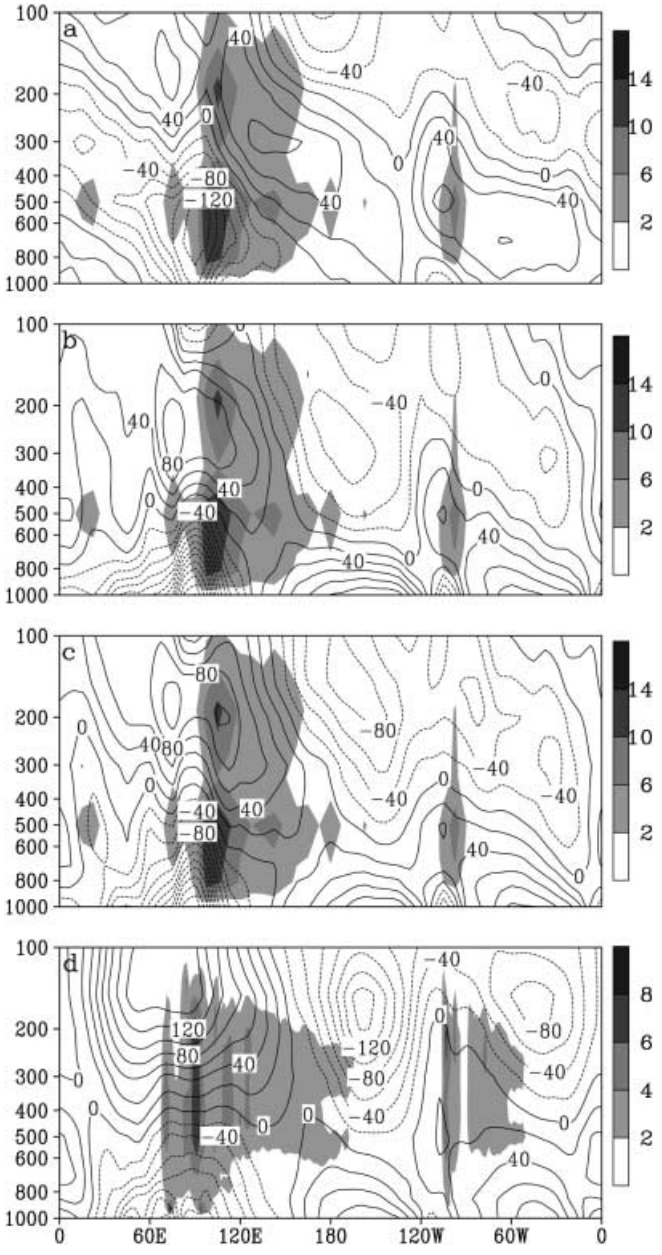

Fig. 8a–d Vertical cross sections of the condensation heating (*shaded*) at 20°N in July and the corresponding geopotential height deviation from the zonal mean at 30°N (*curves*). **a** Average of the last 12-month results from experiment LH3. **b** Is same as **a** but for SHLH. **c** Shows the 16 year average from CON and **d** the average from the NCEP/NCAR reanalysis data for 1980–95. Contour interval is 20 gpm. The boundaries of the *shading* show the heating rate of 2, 6, 10, 14 Kd^{-1} in **a–c**, and 2, 4, 6, 8 Kd^{-1} in **d**

For comparison purposes, the vertical cross section along 30°N of the geopotential height deviations from zonal means calculated from the NCEP/NCAR reanalysis data is given in Fig. 8d. The strength of the SAA at 200 hPa is 100 to 120 gpm, and that of the SAWP in the middle troposphere (500 hPa) is less than 20 gpm. Near the surface, the center of the subtropical anticyclone over the northern Pacific (SANP) is 90 gpm. In LH3 (Fig. 8a), the SAA center is only 60 gpm. The SAWP strength is as high as 40 gpm at 500 hPa. The strength of the SANP is less than 20 gpm. Thus in LH3, the forced SAA and SANP are too weak, and the SAWP is too strong. There must be a mechanism by which the SAA and SANP can be strengthened, and the SAWP weakened.

4.3 Influences of surface sensible heating and seasonal cycle

According to the studies of Wu et al. (1997a), Wu and Zhang (1998), and Ye and Wu (1998) surface sensible heating in summer over the Tibetan Plateau is a key factor in the formation of the anticyclone over the plateau. Wu et al. (1999) also showed that sensible heating is very important for the formation of the SANP. Since sensible heating (SH) is produced by boundary turbulent diffusion, the level of its maximum heating is near the surface. Above this level, sensible heating decreases with height. Thus according to Eq. (5), the steady response of the atmosphere to SH can be approximated as

$$\vec{V}\cdot\nabla\zeta_z+\beta v\propto\frac{f+\zeta}{\theta_z}\frac{\partial Q_{SH}}{\partial z}<0,\quad \theta_z\neq 0\ . \tag{12}$$

In the lower layer, the subtropics is the interface of westerly flow to the north and easterly flow to the south where $u\approx 0$, and the horizontal advection is weak. Due to the β-effect, northerly flow should be forced above the heating source. As a result, the zonal symmetric subtropical anticyclone belt is disturbed, with an anticyclone appearing to the west of the heating region and a cyclone to its east. However, since the background temperature is warm in the south and cold in the north, the upper level is then predominated by westerly flow. According to Eq. (12), advection makes the subtropical anticyclone appear downstream of the heating region and a cyclone upstream of the heating region. This discussion can be used to explain the disposition between the strong land-surface sensible heating along the western coast of northern America in summer and the circulations over the eastern Pacific-North America area and has been confirmed by a series of numerical experiments (Liu 1998; Liu et al. 1999).

Since in the lower troposphere the geopotential height deviation forced by sensible heating is out of phase with that forced by condensation heating, when these two kinds of forcing act together, some compensation in the forced geopotential height may be anticipated. Therefore, the too strong SAWP and too weak SANP in LH3 must be related to the neglect of the effects of sensible heating. In the next experiment LHSH, in addition to the same orography and latent heating as in LH3, surface sensible heating and the associated vertical heat diffusion are also turned on. This experiment is integrated for the same period as in the LH3 experiment and its steady results are shown in Fig. 8b. Comparing Fig. 8b with a, we see that sensible

heating strengthens the SAA in the upper troposphere. This indicates that both the land-surface sensible heating and condensation heating are important to the nature of the SAA. In the middle troposphere, sensible heating reduces the geopotential height over oceans and weakens the SAWP. Near the surface, it intensifies greatly the SANP and the subtropical anticyclone over the North Atlantic. Consequently, the cross section of circulation pattern shown in Fig. 8b is closer to that from the reanalysis data (Fig. 8d).

All of these experiments are perpetual July experiments with the July latent heating kept unchanged. This kind of experiment is different from that with actual seasonal cycle. In order to see how the seasonal cycle of diabatic heating affects the circulation pattern, the July mean cross section of geopotential height derived from the control experiment (CON) is plotted in Fig. 8c. They are very similar to the results from the perpetual July experiment SHLH (Fig. 8b). Thus the use of perpetual experiments in understanding the mechanism of the subtropical anticyclone formation is validated. The effects of seasonal variation are to weaken the pressure systems in the lower troposphere and to strengthen the systems in the upper troposphere. Therefore, the simulated circulation in CON is much closer to the observations shown in Fig. 8d.

5 Interannual variations of condensation heating and subtropical circulation

Equations (9) and (10) and the corresponding experiment results presented all show that condensation heating generates southerlies in the lower troposphere and northerlies in the upper troposphere. This cause-result relation should manifest itself year by year, and be able to be detected from observations. However, atmospheric circulation is influenced not only by condensation heating, but also by other factors. This is particularly true in the lower troposphere where, as discussed in last section, surface sensible heating exerts very strong impacts. To limit the interference of surface sensible heating to a larger extent, 200 hPa circulations obtained from the NCEP/NCAR reanalysis data are retrieved for the following study. Two indices are designed to study the relation in July between the 200 hPa SAA and the condensation heating (CO) of the Asian monsoon. The first index is the northerly index that is defined as the summation of the grid-point meridional velocity that is less than -7.5 m s^{-1} over the area of 15°N–50°N and 110°E–170°W at 200 hPa. The second index is the CO index. To derive this index, firstly the accumulated CO (including large-scale and convective condensation heating) from level $\sigma = 0.5017$ to $\sigma = 0.2101$ at each grid point is calculated and defined as $\sum CO$. Then the summation over the Asian monsoon area (14°N–36°N and 90°E–dateline) of the $\sum CO$ that is more than 30 °C d^{-1} at one grid point is defined as the CO index. It is calculated from the July mean NCEP/NCAR reanalysis data on the T62 base.

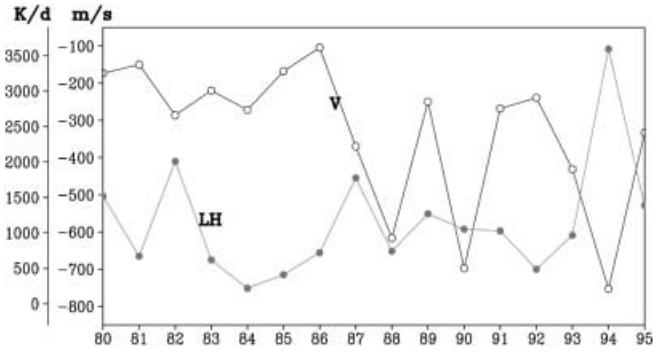

Fig. 9 Interannual variations of the July northerly index (ms^{-1}, the *curve with* ○) and the condensation heating index (°C d^{-1}, the *curve with* ●). See text for definitions

In Fig. 9 the interannual variations of these two indices are shown. The negative correlation between the two curves is apparent. Their correlation coefficient is −0.525, which is already above the 95% significance level (0.497). Considering the possible interference from the effects of sensible heating as well as the mechanical and thermal forcing of the Tibetan Plateau, we may regard this correlation as significant. It provides good evidence that the formation of the SAA in summer is, to a great extent, a result of the condensation heating associated with the Asian summer monsoon.

6 Conclusions and discussion

Based upon the complete vorticity equation and a series of numerical experiments, the atmospheric response to the subtropical heating is investigated in this study. Results show that strong condensation latent heating can intensify westerlies to the north and easterlies to the south, while the zonal advection crossing the heating center is weak. It is the vertical heating profile that causes the atmospheric response in the lower troposphere to be out of phase with that in the upper troposphere. In the lower troposphere the forced anticyclone appears on the eastern side of the heating region; whereas in the upper troposphere, it appears on the western side of the heating region. Results also show that the formation of the SAWP is mainly due to the condensation heating associated with the Asian summer monsoon, but modified to some extent by surface sensible heating. As to the formation of the SAA, it is partly due to the monsoon condensation heating and partly due to the sensible heating over the Tibetan Plateau.

An important phenomenon revealed in this study is that due to horizontal gradient of the condensation heating, there exists an extra negative vorticity forcing to the north of the condensation heating region. It makes the pronounced anticyclone and cyclone forced by the heating located along the latitudes to the north of the

heating region. Moreover, the subtropical heating can generate Rossby wave trains via energy dispersion. These wave trains possess quasi-barotropic structure and strongly affect the flow pattern in the extra-tropics.

Based on data diagnosis, Nitta (1987) and Huang and Li (1989) found that enhanced convection over the warm pool region can generate a positive anomaly in geopotential height to its north, and cause the SAWP to be shifted northward. Their results are similar to that shown in Fig. 4c, and can be well explained by the associated negative vorticity forcing to the north of the enhanced convective heating regions.

By diagnosing the interannual variations based on the NCEP/NCAR reanalysis data, it is found that in July the condensation heating of the Asian monsoon and the northerlies to the east of the 200 hPa SAA is significantly correlated. This therefore verifies and supports the theory that condensation heating along the subtropical area is important for the formation of the subtropical anticyclones in the boreal summer.

In some studies, the SANP and the SAWP are regarded as one circulation system. In these studies the SAWP is considered as the westward extension of the SANP, and its movement is forecasted by tracing the variations of the SANP. However, the results of Liu (1998) and this study show that their formation mechanisms are different. The SANP is forced dominantly by the land-surface sensible heating over North America, whereas the SAWP is forced mainly by the monsoon condensation heating. They cannot be treated as one system.

Traditionally, the SAWP is regarded as a control system, and the movements around the SAWP of typhoon, rainfall belt, and westerly trough are monitored by the SAWP. This idea has been extended to climate studies. However, this study shows that, at least on the climatic time scale, SAWP is greatly influenced by the monsoon condensation heating. Therefore the relationship between the SAWP and the weather/climate systems around it is not a matter of principal and subordinate forces but interactive ones. Further studies on this interaction will improve our understanding on subtropical anticyclone dynamics and contribute to progress in short-term climate prediction.

Acknowledgements The authors wish to thank Professor WL Gates and two anonymous reviewers for their thoughtful and constructive comments. This research is supported jointly by the National Key Programme for Developing Basic Sciences (G1998040900-part 1), and by the Natural Science Foundation of China under Grant 49905002, 49635170 and 49825504, Chinese Academy of Sciences Grant "Hundred Talents" for "Validation of Coupled Climate Models".

References

Ertel H (1942) Ein neuer hydrodynamische Wirbelsatz. Meteor Z 59: 277–281

Flohn H (1957) Large-scale aspects of the "summer monsoon" in South and East Asia. J Meteorol Soc Japan (75th Ann Vol), 180–186

Gill AE (1980) Some simple solutions for heat-induced tropical circulation. QJR Meteorol Soc 106: 447–662

Hoskins BJ (1986) Diagnosis of forced and free variability in the atmosphere. In: Cattle H (ed) Atmospheric and oceanic variability. James Glaisher House, Bracknell UK, pp 57–73

Hoskins BJ (1996) On the existence and strength of the summer subtropical anticyclones. Bull Am Meteorol Soc 77(6): 1287–1292

Hoskins BJ, Karoly D (1981) The steady linear response of a spherical atmosphere to thermal and orographic forcing. J Atmos Sci 38: 1179–1196

Huang SS, Yue TH (1962) On the structure of the subtropical highs and same associated aspects of the general circulation of atmosphere. Acta Meteorol Sinica 31: 339–359 (in Chinese)

Huang RH, Li L (1989) Numerical simulation of the relationship between the anomaly of the subtropical high over East Asia and the convective activities in the western tropical Pacific. Adv Atmos Sci 6: 202–214

Krishnamurti TN (1973) Tibetan High and upper tropospheric tropical circulation during northern summer. Bull Am Meteorol Soc 54: 1234–1249

Li MC, Luo ZX (1988) Effects of moist process on subtropical flow patterns and multiple equilibrium states. Sci Sinica (B) 31: 1352–1361

Liu H, Wu GX (1997) Impacts of land surface on climate of July and onset of summer monsoon: a study with an AGCM plus SsiB. Adv Atmos Sci 14: 289–308

Liu YM (1998) Impacts of spatially inhomogeneous diabatic heating on the formation of subtropical anticyclone in boreal summer. PhD Thesis, Institute of Atmospheric Physics, Chinese Academy of Sciences, pp 135 (in Chinese)

Liu YM, Liu H, Liu P, Wu GX (1999) The effect of spatially non-uniform heating on the formation and variation of subtropical high. Part II: land surface sensible heating and east pacific-north America subtropical high. Acta Meteorol Sinica 57: 385–396 (in Chinese)

Manabe S, Smagorinsky J, Strickler RF (1965) Simulated climatology of general circulation model with a hydrologic cycle. Mon Weather Rev 93: 769–798

Nitta T (1987) Convective activities in the tropic western Pacific and their impact on the Northern Hemisphere summer circulation. J Meteorol Soc Japan 65: 373–390

Peixoto JP, Oort AH (1991) Physics of climate. American Institute of Physics Press, New York, pp 520

Peng GB (1987) Connections of the west Pacific subtropical high and snow hydroclimatical regions in China with Antarctic ice-snow indices. Meteor Atmos Phys 37: 61–71

Phillips NA (1973) Principles of large-scale numerical weather prediction. In: Morel P (ed) Dynamic meteorology. D. Reidel, Dordrecht, Holland, pp 1–96

Rodwell MR, Hoskins BJ (1996) Monsoons and the dynamics of deserts. QJR Meteorol Soc 122: 1385–1404

Samel AN, Wang WC, Liang XZ (1999) The monsoon rainfall over China and relationships with the Eurasian circulation. J Clim 12: 115–131

Smagorinsky J (1953) The dynamical influence of large-scale heat sources and sinks on the quasi-stationary mean motions of the atmosphere. QJR Meteorol Soc 79: 342–366

Shi GY (1981) An accurate calculation of the infrared transmission function of the atmospheric constituents. PhD Thesis, Tohoku University of Japan, pp 191

Tao SY, Zhu FK (1964) Variation of the 100 hPa flow pattern in South Asia in summer and the movement of the subtropical anticyclone over the western Pacific. Acta Meteorol Sinica 34(4): 385–394 (in Chinese)

Tao SY, Chen L (1987) A review of recent research on the East Asia summer monsoon in China. In: Krishnamurti (ed) Monsoon meteorology, Oxford University Press, Oxford, UK, pp 60–92

Wang B (1996) On the radiation transfer models for climate simulation. PhD Thesis, Institute of Atmospheric Physics, Chinese Academy of Sciences, pp 92 (in Chinese)

Wu GX, Liu HZ (1998) Vertical vorticity development owing to down-sliding at slantwise isentropic surface. Dyn Atmos Ocean 27: 715–743

Wu GX, Zhang YS (1998) Tibetan Plateau forcing and the timing of the monsoon onset over South Asia and the South China Sea. Mon Weather Rev 126: 913–927

Wu GX, Liu YM, Liu P (1999) The effect of spatially non-uniform heating on the formation and variation of subtropical high. Part I: scale analysis. Acta Meteorol Sinica 57: 257–263 (in Chinese)

Wu GX, Liu H, Zhao YC, Li WP (1996) A nine-layer atmospheric general circulation model and its performance. Adv Atmos Sci 13: 1–18

Wu GX, Li WP, Guo H, Liu H (1997a) Sensible heating-driving air pump of the Tibetan Plateau and the Asian summer monsoon. In: Ye DZ (ed) Memorial Volume of Prof. Zhao JZ. Science Press, Beijing, pp 116–126 (in Chinese)

Wu GX, Zhang XH, Liu H, Yu YQ, Jin XZ, Guo YF, Sun SF, Li WP, Wang B, Shi GY (1997b) Global ocean-atmosphere-land system model of LASG (GOALS/LASG) and its performance in simulation study. Q J Appl Meteorol 8: 15–28 (in Chinese)

Xue YK, Sellers PJ, Kinter JL, Shukla J (1991) A simplified biosphere model for global climate studies. J Clim 4: 345–364

Ye DZ, Gao YX (1979) Meteorology of the Qinghai-Xizang Plateau. Chapter 1. Chinese Science Press, Beijing, pp 178

Ye DZ, Wu GX (1998) The role of the heat source of the Tibetan Plateau in the general circulation. Meteorol Atmos Phys 67: 181–198

Ye DZ (also Yeh TC), Lo SW, Chu BC (1957) On the heat balance and circulation structure in the troposphere over the Tibetan Plateau and its vicinity. Acta Meteorol Sinica 28: 108–121 (in Chinese)

Zeng QC (1963) Characteristic parameter and dynamical equation of atmospheric motions. Acta Meteorol Sinica 33: 472–483 (in Chinese)

Zhang R, Shi HS, Yu SH (1995) A study of non-linear stability of the western Pacific subtropical high. Chinese J Atmos Sci 19: 687–700 (in Chinese)

Zhang XH, Chen KM, Jin XZ, Lin WY, Yu YQ (1996) Simulation of thermohaline circulation with a twenty-layer oceanic general circulation model. Theor Appl Climatol 55: 65–88